Accepted Manuscript
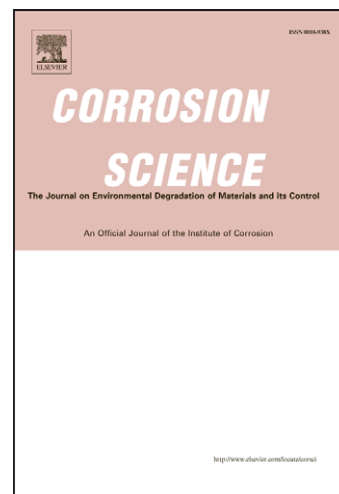
Hydrogen transport and embrittlement in 300m and aermet100 ultra high strength steels

D. Figueroa, M.J. Robinson

HYDROGEN TRANSPORT AND EMBRITTLEMENT IN 300M AND AERMET100 ULTRA HIGH STRENGTH STEELS

D.Figueroa[+] & M.J.Robinson
School of Applied Sciences
Cranfield University, Bedford, UK

[+] present address: Corus Strip Products UK, South Wales, UK

Abstract
This paper describes how hydrogen transport affects the severity of hydrogen embrittlement in 300M and AerMet100 ultra high strength steels. Slow strain rate tests were carried out on specimens coated with electrodeposited cadmium and aluminium-based SermeTel 1140/962. Hydrogen diffusivities were measured using two-cell permeation and galvanostatic charging methods and values of 8.0×10^{-8} and $1.0 \times 10^{-9} cm^2 s^{-1}$ were obtained for 300M and AerMet100, respectively. A two-dimensional diffusion model was used to predict the hydrogen distributions in the SSR specimens at the time of failure. The superior embrittlement resistance of AerMet100 was attributed to reverted austenite forming around martensite laths during tempering.

Keywords;   steel (A), hydrogen permeation (B), galvanostatic (B), hydrogen embrittlement (C)

INTRODUCTION

When high strength steels are protected from corrosion by a sacrificial metallic coating there is an increased risk of failure by hydrogen embrittlement and this can occur in two ways. First, if the coating is applied by electrodeposition a small proportion of the plating current produces hydrogen that is reversibly trapped in the coating and then slowly absorbed by the steel. This hydrogen can lead to delayed failure of high strength steel under load and it is the usual practice to bake such components for up to 24 hours at 200°C to remove the hydrogen [1,2]. Failure resulting from hydrogen uptake during electroplating is referred to as direct embrittlement.

Second, hydrogen can also be absorbed when a sacrificial coating corrodes in service. In this case, exposed areas of the steel substrate act as cathodic sites where hydrogen is generated by the reduction of water. If this hydrogen is absorbed in sufficient quantities it can also lead to failure of high strength steel and this process is termed hydrogen re-embrittlement [3,4].

The composition of the sacrificial coating determines the concentration of hydrogen produced at the surface of the exposed steel substrate, with more active metals leading to higher hydrogen concentrations. The structure of the coating is also a factor as a

dense layer acts as an effective barrier, whereas a cracked or porous one provides a short circuit path to the steel surface for hydrogen uptake to occur. The effects of composition and structure of different sacrificial coatings on direct embrittlement and re-embrittlement of high strength steels have been discussed in a previous paper [4].

The extent of hydrogen embrittlement generally increases with the tensile strength of the steel [5] but the grain size and the phases present in the microstructure also have an important influence by affecting hydrogen trapping and thereby controlling the rate of hydrogen uptake [6]. This paper compares the hydrogen embrittlement and re-embrittlement of two ultra high strength steels coated with electroplated cadmium and a non-electrolytic aluminium-based SermeTel 1140/962 coating. Slow strain rate tensile tests were performed to measure the extent of embrittlement in each experimental condition and the results are discussed in terms of the hydrogen permeation rates in the two materials, determined by two electrochemical techniques. Finally, mathematical modeling has been used to relate the uptake of hydrogen in the two steels to the fractography observed in the tensile tests.

METHODS

Materials

The first steel was 300M (UNS K44220) produced by vacuum arc melting. It was tested in the hardened condition by austenitizing at 870 °C and oil quenching to room temperature, followed by a double tempering at 315°C to give a tensile strength of 2250 MPa. The second steel was AerMet100 (UNS K92580), which is a high alloy steel containing nickel, cobalt and chromium. This was heat treated by austenitising at 843°C, oil quenching to room temperature followed by 1 hour at -73°C to transform retained austenite and finally tempered at 485°C for 5 hours. The resulting tensile strength was 2100 MPa. The chemical compositions of both alloys are shown in Table 1.

The microstructures of the 300M and AerMet100 steels consisted of lath/plate martensite with M_7C_3, $M_{23}C_6$ and ε-carbides distributed within the matrix and at the boundaries [7-9]. In 300M, examination in a SEM showed that some retained austenite was present at prior austenite grain boundaries. Retained austenite was also visible in AerMet100 and, in addition, a thin film of reverted austenite had formed at lath/plate boundaries during the final tempering treatment. In each case, the quantity of austenite was too low to be detected by x-ray diffraction. The same microstructure has been reported in the literature for AerMet100, following similar heat treatments [10,11]. The carbides, and the retained and reverted austenite are all known to act as strong hydrogen traps [8,12] and their significance in the microstructure will be discussed in a later section.

Hydrogen diffusivities

Two methods were used to measure the hydrogen diffusion coefficient, D, of the two steels. The hydrogen permeation technique was suitable for 300M steel but was insufficiently sensitive to measure the lower diffusion coefficient of AerMet100. Instead, a galvanostatic charging technique was adopted, which was satisfactory for both materials.

Hydrogen permeation technique The measurements were made using the double cell permeation technique of Devanathan and Stachurski [13]. A membrane of the steel, 1mm thick was polished to a 1μm diamond finish and held between two electrochemical cells with an exposed surface area of 50.3 cm^2 on each side. Both cells contained an electrolyte of 0.2 M NaOH solution. Prior to hydrogen charging, the membrane was depleted of residual hydrogen by holding the exit surface at a potential of -0.094 V (SCE) until the current density was lowered to 0.01μAcm^{-2}. Charging was then carried out on one side only by maintaining the entry surface at a constant potential of -1.250 V (SCE) to promote hydrogen generation and uptake. The hydrogen that diffused through the membrane was oxidised and detected on the exit side. After an interval known as the breakthrough time, t_b, the oxidation current displayed a rising transient and eventually reached a steady state value, J_∞.

$$J_\infty = \frac{D\,C_o}{L} \qquad\qquad (1)$$

Where the D is the hydrogen diffusion coefficient, C_o is the constant hydrogen concentration at the charging side of the membrane, and L is the membrane thickness. The aim of the experiment was to measure the hydrogen diffusion coefficient of the steel, which was calculated from the breakthrough time using equation (2)

.

$$t_b = \frac{L^2}{15.3\,D} \qquad\qquad (2)$$

In this case, the C_o value in the charging side of the membrane was not of interest as it was not required to determine D. Using a potential of -1.250 volts (SCE) and 0.2M NaOH electrolyte gave a high rate of hydrogen charging and avoided corrosion on the entry side of the steel membrane.

Galvanostatic method The electrochemical principle of the method has been clearly reviewed by Wen et al [14] and its application is reported in several other studies [15-17]. The technique involves using a current pulse to cathodically charge a thin sample of the material from both sides in a two-electrode cell and record the cell potential difference, E, as a function of time. The charging current produces a constant flux of hydrogen at the electrolyte/metal interface, $x = 0$, and the increasing cell voltage that is recorded provides a direct measure of the hydrogen activity in the steel at the interface. Under these experimental conditions the initial and boundary conditions for a sample of thickness 2L, charged from both sides, are:

$$C = C_0 \qquad\qquad 0 \le x \le L, \qquad\qquad t = 0 \qquad\qquad (3)$$

$$-D\frac{\mathrm{d}C}{\mathrm{d}x} = \frac{I}{zFS} \qquad\qquad x = 0, \qquad\qquad t > 0 \qquad\qquad (4)$$

$$\frac{\mathrm{d}C}{\mathrm{d}x} = 0 \qquad\qquad x = L, \qquad\qquad t \ge 0 \qquad\qquad (5)$$

3

where C, t, D and x are the molar hydrogen concentration, diffusion time, hydrogen diffusion coefficient and distance from the metal surface, respectively, and I, S, z and F are the charging current, sample area, charge number of the ion reduced in the electrolyte (ie H^+) and Faraday's constant

The solution of Fick's second law for one dimensional diffusion can be expressed as either error function or trigonometric series. It can be shown that for very short times, $(t << L^2/D)$, the concentration of hydrogen at the interface (as measured by the cell potential difference) can be approximated by the first term of the error function series. In this condition, the potential difference, E, is linearly related to $t^{1/2}$, as shown in equation (6). The gradient $dE/dt^{1/2}$ can be obtained from the gradient of the graph of E vs $t^{1/2}$.

$$\frac{dE}{dt^{1/2}} = \frac{2\,I\,Vm}{z\,F\,S\,(\pi\,D)^{1/2}}\left(\frac{dE}{d\delta}\right) \quad \text{if } t << \frac{L^2}{D} \tag{6}$$

where Vm is the molar volume of the steel sample and $dE/d\delta$ is the change in cell voltage with change in hydrogen concentration.

At longer times, $(t > L^2/D)$, the surface hydrogen concentration is approximated by the first two terms of the infinite trigonometric series and dE/dt is linearly related to the diffusion time, as given in equation (7).

$$\left(\frac{dE}{dt}\right) = \frac{I\,Vm}{F\,S\,L}\left(\frac{dE}{d\delta}\right) \quad \text{if } t > \frac{L^2}{D} \tag{7}$$

Equations (6) and (7) can be combined to eliminate $dE/d\delta$ and the diffusion coefficient is then calculated from the gradients $dE/dt^{1/2}$ and dE/dt at short and long times, respectively.

$$D = \left(\frac{2L\dfrac{dE}{dt}}{\pi^{1/2}\dfrac{dE}{dt^{1/2}}}\right)^2 \tag{8}$$

In the practical measurements, the 300M steel sample was 2mm thick (ie $2L$=2mm) with a charging area of $1.44cm^2$ and the AerMet100 sample was 1mm thick ($2L$=1mm) with an area of $2.64cm^2$. Both were polished to a $1\mu m$ finish with diamond paste and the edges were protected with Lacomit. In each case, a platinum counter electrode was used and the current density was 1 mAcm^{-2}. The electrolyte was 0.2M NaOH, with the addition of 1g l^{-1} of thiourea as a recombination poison to ensure that hydrogen generated at the surface entered the metal rather than escaping as bubbles.

Hydrogen embrittlement tests

The two high strength steels were machined in the form of tensile specimens, with a gauge length of 25 mm and diameter of 2.75 mm. Some of the tensile specimens were coated with 8 microns of electrodeposited cadmium and others were coated with SermeTel 1140/962 by Sermatech International Inc in Lincoln, UK. This coating consisted of densely packed aluminium particles in a chromate/phosphate inorganic binder and was applied as two spray coats, each being cured at 315°C to give a total thickness of 70 microns. As the process was non-electrolytic it was not expected that these coatings would cause direct embrittlement of the steel substrates. A modified polyurethane top-coat was applied to enhance the corrosion resistance and barrier properties of the coating.

The extent of direct hydrogen embrittlement and re-embrittlement in the coated specimens was assessed by performing slow strain rate (SSR) tests. Initial tests were carried out in air on uncoated specimens to provide a baseline for comparison. The strain rate was $9.7 \times 10^{-7} \text{s}^{-1}$ and four specimens were tested for each experimental condition. Some of the cadmium plated specimens were tested in the as-plated condition. (They were stored in liquid nitrogen within 8h of plating to immobilize hydrogen in the cadmium and the steel until the test could be carried out). Other plated specimens were tested after being given a de-embrittlement treatment by baking for 24h at 200°C. Further tests investigated the effects of corrosion of the cadmium coating by surrounding the gauge length of plated and baked specimens with a cell containing 3.5% NaCl solution to simulate service conditions and establish representative surface hydrogen concentrations. In these tests the gauge length was scribed to remove the coating and expose the substrate over a width of 1 mm. Similar tests were performed on specimens coated with SermeTel 1140/962 to measure the re-embrittlement caused by corrosion of this aluminium-based coating.

Embrittlement index In each case, the time to failure of a coated tensile specimen (t_c) was recorded and compared with the mean failure time (t_a) of uncoated specimens tested in air. The embrittlement index (EI) was calculated as follows;-

$$EI = 1 - t_c/t_a \qquad (9)$$

RESULTS

Hydrogen diffusivities

A typical transient for 300M from the two-cell permeation technique is shown in Figure 1. The mean breakthrough time for three replicate experiments was 1.9 ± 0.06 hours and this corresponded to a hydrogen diffusion coefficient of $9.6 \pm 0.3 \times 10^{-8}$ cm^2s^{-1} from equation (2). It was evident that AerMet100 had a much lower diffusivity as the current transient was very small and the breakthrough time and steady state current were difficult to detect (equation (1)).

The results of the galvanostatic method for both 300M and AerMet100 are shown in Figures 2. The plot of cell potential difference against time displays a parabolic shape for short charging times, $t << L^2/D$, followed by a linear region at longer times when $t > L^2/D$. The corresponding graphs of E vs. $t^{1/2}$ and E vs. t are shown in Figures 3 and

4, respectively and their gradients were used to calculate the hydrogen diffusion coefficients from equation (8).

The hydrogen diffusion coefficients for 300M and AerMet100 steels were 8.0×10^{-8} and $1.0 \times 10^{-9} \text{cm}^2\text{s}^{-1}$ respectively and the results for the two methods are summarised in Table 2.

Hydrogen embrittlement testing
Hydrogen embrittlement tests on high strength steel often display a range of times to failure when carried out under apparently identical experimental conditions. This is due to differences in the number, size and distribution of micro structural flaws within the specimen at which hydrogen accumulates and leads to fracture. In addition, flaws and lack of uniformity in the sacrificial coating will lead to differences in the rate of hydrogen uptake by the steel and this too will affect the failure time. In this work, Weibull statistics was used to display the probability of each of the four replicate specimens in each group surviving for a specific time before then failing by hydrogen embrittlement or re-embrittlement.

Weibull model of failure times It can be shown that for a Weibull model the probability, P_s, of a specimen not failing within time, t, is given by;-

$$P_s = 1 - P_f = e^{-xt} \qquad (10)$$

Where P_f is the probability of failure and x is a shape parameter termed the Weibull slope [18-20]. In the present context, x represents the probability per unit time that during time, t, a crack will form in the specimen of sufficient size to cause failure. The value of x can be obtained from the negative gradient of a graph of $\ln P_s$ against t. In practice, there is a minimum time, t_i, for a crack to initiate and the graph is displaced along the time axis by this amount. (When $P_s = 1$, then $\ln P_s = 0$ and $t = t_i$).

In this case, Equation (10) can be modified to include t_i.

$$P_s = 1 - P_f = e^{-x(t - t_i)} \qquad (11)$$

Student t-test In addition to the Weibull model, the Student t-test [21] for small sample sizes was used to determine whether a set of failure time data, from the four replicate specimens, was significantly different from other sets of data measured under different experimental conditions, or whether they should be considered to be part of the same overall population.

The test compared the means of the two data sets, m_1 and m_2, to calculate the test statistic, t, as follows;

$$t = \frac{(m_1 - m_2)}{s\sqrt{(1/n_1 + 1/n_2)}} \qquad (12)$$

6

where n_1 and n_2 were the number of failure times in each data set (in this case $n_1=n_2=$ 4) and s was found from the standard deviations for the two sets.

$$s^2 = \frac{s_1{}^2 + s_2{}^2}{2} \qquad (13)$$

The test statistic was then compared with tabulated values of a t-distribution for a 95% confidence level with 6 degrees of freedom ($n_1 + n_2$ -2). If the test static was less than the t-distribution then it could be concluded with this confidence level that the two data sets were part of the same overall population (the null hypothesis).

Slow strain rate tests The slow strain rate test results for 300M and AerMet100 specimens, tested in air and when cadmium coated and exposed to 3.5% NaCl solution, are shown in Figures 5 and 6. The mean failure times for the four replicate specimens in each condition and the corresponding embrittlement indices are compared in Table 3. 300M displayed much more direct embrittlement than AerMet100 and when electroplated with cadmium its embrittlement index, EI, was 0.54, compared to only 0.05 for AerMet100. Post-plating baking the cadmium plated specimens at 200°C was effective in removing hydrogen from the microstructure and the mechanical properties were almost completely recovered to give an EI for 300M of 0.04. Corrosion of the cadmium coating in 3.5% NaCl solution caused significant re-embrittlement of 300M and an EI of 0.16. However, AerMet100 displayed no re-embrittlement in 3.5% NaCl solution. Its lower susceptibility was attributed to the distribution of phases in its microstructure, as discussed in a later section.

The results for the re-embrittlement tests on the aluminium-based SermeTel 1140/962 coated specimens are also shown in Figures 5 & 6. The open circuit potential of SermeTel 1140/962 in 3.5% NaCl solution (-0.76 V (SCE)) was very close to that of electrodeposited cadmium (-0.75 V (SCE)) yet it led to greater re-embrittlement of 300M, with an EI of 0.27. The structure of the coating is believed to be an important factor affecting hydrogen uptake, in addition to its electrochemical potential [4]. In contrast, AerMet100 specimens showed no reduction in failure times when tested in 3.5% NaCl solution. In fact, there was a small increase in the mean failure time, as shown in Table 3, which resulted in a negative value for the calculated embrittlement index. It is possible that the baking treatment at 315°C to cure the coating may have slightly affected the mechanical properties of the steel. However, this temperature was well below the tempering temperature of the material (485°C for 5h) and the Student-t test showed, with a 95% confidence level, that the coated and uncoated AerMet100 specimens could not be considered to belong to different statistical populations.

Appearance of the fracture surfaces
After the SSR tests, the fracture surfaces were examined in a scanning electron microscope. The different failure modes were carefully mapped across the surfaces and are shown schematically for each material in Figures 7 and 8. The 300M specimens had very little reduction in area due to their high level of embrittlement, whereas the AerMet100 fractures were more ductile and necking had occurred. In 300M, a brittle fracture had initiated at a single point at the edge of each specimen and

propagated inwards until the stress on the remaining section exceeded the UTS, whereupon it then failed in a ductile manner by microvoid coalescence. The mean depth of brittle fracture was 1.0mm. The initial brittle fracture was intergranular, suggesting that the applied stress had been relatively low [22], and this changed to a transgranular cleavage mode as the crack grew in length and the stress increased (Figure 9). In contrast, all the regions of brittle fracture in AerMet100 specimens were transgranular cleavage. They had initiated from many sites around the circumference but had propagated only a short distance (mean depth of 0.13mm) before the final ductile failure occurred.

DISCUSSION

Conditions for embrittlement in SSR tests

For hydrogen embrittlement failures to occur in SSR tests, two principal conditions need to be met. The applied stress and the concentration of absorbed hydrogen at the specimen surface must both exceed threshold values for a brittle crack to initiate [23,24]. While the stress increased slowly during the SSR test, hydrogen was diffusing into the specimen from the reservoir of hydrogen in the unbaked cadmium coating [25]. Eventually the stress exceeded the threshold value and a brittle crack initiated. The crack then propagated rapidly towards the centre of the specimen, as the material in this region contained more than the threshold hydrogen concentration. When the stress on the remaining cross-section reached the UTS, a ductile overload failure occurred.

Clearly, the depth of the brittle region observed on the fracture surface is a measure of the depth to which hydrogen had diffused in that specimen. Therefore, by determining this distance it is feasible to model hydrogen diffusion across the section and to calculate the corresponding diffusion coefficients [26] which can then be compared with those obtained from the electrochemical measurements. In practice, some hydrogen would have diffused further than the embrittled region, as the concentration at the crack tip is required to reach the threshold value. Therefore, the diffusion coefficients assessed from the fracture surfaces should be regarded as minimum values. This model does not preclude any specific crack tip mechanism for hydrogen embrittlement [27]. For example, the slip softening mechanism [28] can explain how, in certain circumstances, crack growth can be accompanied by the enhanced generation and mobility of dislocations and an observed lowering of the stress required for plastic deformation. However, such crack propagation would still require absorbed hydrogen to have diffused to sufficient depth below the surface and for a threshold concentration to have been exceeded.

Modelling hydrogen uptake by the SSR specimens

The case of two-dimensional, radial diffusion in a cylinder has been considered. The rate of hydrogen uptake at the surface, F, is dependent on the hydrogen diffusion coefficient of the steel, D, and the concentration gradient, dC/dx, according to Fick's first law of diffusion [29].

$$F = -\,D\,dC/dx \qquad (14)$$

Before the start of the test the residual hydrogen concentration in the specimen, C_1, was assumed to be zero and as soon as hydrogen charging began the surface concentration took on a value, C_0, and remained constant. These boundary conditions, which apply for the case of potentiostatic charging [13] are defined below, where r is the distance from the centreline of a specimen of radius a.

$$C = C_1 = 0, \quad 0 < r < a, \quad t = 0 \qquad (15)$$

$$C = C_0, \quad r = a, \quad t \geq 0 \qquad (16)$$

As the test proceeded, the hydrogen content of the steel increased such that the concentration gradient ($C_0 - C$) was progressively reduced and the rate of hydrogen uptake decreased also. The solution of the diffusion equation for the case of hydrogen transport into a solid cylindrical specimen [29,30], of infinite length, is given in equation (17).

$$\frac{C - C_1}{C_0 - C_1} = 1 - 2\sum_{n=1}^{\infty} \frac{\exp(-\alpha_n^2 Dt / a^2) J_0(r\alpha_n / a)}{\alpha_n J_1(\alpha_n)} \qquad (17)$$

Where $\alpha_n, n = 1,2,......$ are roots of $J_0(\alpha) = 0$, the Bessel function of zero order and $J_1(\alpha)$ is the Bessel function of the first order. The series is convergent and was evaluated for the first 150 Bessel roots. For the initial condition, $C_1 = 0$, the equation simply gives the concentration C/C_0.

Minimum rates of hydrogen uptake
Figure 10 shows the least depth to which hydrogen could have penetrated into the cadmium plated, but unbaked, 300M SSR specimens in the mean failure time of 14.5 hours, to explain the observed failures. The graph represents the hydrogen concentration, C, as a proportion of the surface concentration, C_o, across the 2.75mm diameter of the specimen, when charged from both sides. In evaluating the series in equation (17), the hydrogen diffusion coefficient has been adjusted so that hydrogen just reached a depth of 1.0mm, which was the mean depth of the embrittled region on the four replicate 300M specimens. For this condition to be satisfied, the diffusion coefficient would need to be 1×10^{-8} cm^{2}s^{-1}, compared to 8.0×10^{-8} cm^{2}s^{-1} measured using the galvanostatic method.

Similar calculations were carried out for AerMet100 such that hydrogen just penetrated 0.13mm from the surface; the mean depth of the embrittled region in cadmium plated specimens of this alloy, as shown in Figure 11. In this case, D needed to be 8×10^{-11} cm^{2}s^{-1}, whereas the measured value was 1×10^{-9} cm^{2}s^{-1}. As the measured diffusion coefficients were the higher values in both steels, it appears that at the time of failure hydrogen had diffused further than the embrittled region, indicating that a significant hydrogen concentration was required at the crack tip for the brittle fracture to propagate.

9

Threshold hydrogen concentrations

Figures 12 and 13 show the hydrogen distribution for each alloy that would be predicted from its failure time and measured diffusion coefficient. For 300M (Figure 12) distributions are shown for a range of times up until failure occurred. For example, at 10440s hydrogen had just penetrated from each side of the specimen to reach the centre (the breakthrough time $t_b=0.04L^2/D$). At failure (52200s), the hydrogen concentration, C/C_o, at a depth of 1.0mm was predicted to be 0.6. That is to say, the concentration was 0.6 of that at the surface due to hydrogen charging from the cadmium coating. This value represents the threshold hydrogen concentration for embrittlement in 300M.

The corresponding hydrogen distribution for AerMet100 at the failure time of 111960s is shown in Figure 13. At the mean embrittlement depth of 0.13mm, the hydrogen concentration is predicted to be 0.4 C/C_o.

Comparison of the embrittlement susceptibilities

The SSRT results indicate that 300M was the more susceptible of the two alloys to direct hydrogen embrittlement from cadmium plating and re-embrittlement from hydrogen generated when the cadmium and aluminium-based sacrificial coatings were corroded. The hydrogen diffusion coefficient was shown to be approximately 80 times higher in 300M than in AerMet100 and it appears that the faster rate of hydrogen uptake in 300M was a major contributory factor in its greater susceptibility in the SSR tests. Whether AerMet100 would display greater embrittlement if more time was available for hydrogen uptake is an interesting point to consider and this could be investigated by performing tests at a slower strain rate to allow more time for diffusion.

A comparison of the threshold hydrogen concentrations, C_{th}, required to propagate a brittle crack (Figures 12 and 13) might suggest that AerMet100 was slightly more susceptible than 300M (C/C_o of 0.4 for AerMet100 and 0.6 for 300M). However, this difference is not thought to be particularly significant. Both steels have tempered martensite in the microstructure and embrittlement of this phase is expected to be similar in each case. In addition, due to the steepness of the hydrogen distribution profile in Figure 13, a small difference in the measured depth of embrittlement in AerMet100 would result in a large difference in the predicted C/C_o value. However, there are features of the microstructure of AerMet100 that explain both its low embrittlement susceptibility and the low hydrogen diffusion coefficient.

The influence of microstructure

Both steels consisted of tempered martensite and the marked difference in the two hydrogen diffusivities is thought to result from the concentration and distribution of trap sites in their microstructures. In particular, the presence of retained and reverted austenite is an important factor [4]. Figure 14 shows that in 300M retained austenite was present at prior austenite grain boundaries, whereas in AerMet100 the austenite was distributed more widely, on both prior austenite boundaries and martensite lath boundaries. Previous work reported similar microstructures in 300M that had received equivalent heat treatments to that used in the present study [8,12]. Ritchie et al [31] showed that the presence of retained austenite was beneficial in controlling hydrogen embrittlement and attributed this to a reduction in the diffusivity of hydrogen due to its high solubility in austenite. In the case of AerMet100, the

10

austenite was thought not to have been retained during quenching but to have formed by partial reversion of martensite during tempering for 5 hours at 485°C [32,33]. Austenite, is known to have a high hydrogen solubility and low hydrogen diffusivity [34] and therefore acts as an effective trap when present in an essentially martensitic microstructure. The hydrogen diffusion coefficient of austenitic stainless steel is reported [35] to be in the range 1.8-8 x 10^{-12} cm^{2}s^{-1} and, although these alloys contain chromium and nickel, this indicates the low rate of diffusion that can be expected in high strength steels when austenite is present. Similarly, it has been reported that the apparent diffusivity of duplex stainless steel containing 44% austenite is reduced by approximately 400 times in comparison with that of a fully ferritic steel, due to hydrogen trapping in the austenite phase [35]. In 300M, austenite retained at prior austenite grain boundaries would have trapped some hydrogen but this would have provided limited benefit as the martensite laths within the grains would have remained vulnerable to embrittlement. In AerMet100, however, the presence of a thin (3nm) but essentially continuous envelope of reverted austenite around the martensite laths has been reported [36] and this lowered the risk of embrittlement in the present work by acting as a very effective barrier to restrict hydrogen transport and prevent a critical hydrogen concentration being reached in the more susceptible martensite phase. The factors affecting hydrogen uptake and embrittlement have been discussed in more detail in a previous paper [4].

Effect of coating type on hydrogen re-embrittlement
It was shown in Table 3 that less re-embrittlement occurred from corrosion of the cadmium coating (EI 0.16) than from that of the SermeTel 1140/962 coating (EI 0.27), although they had very similar open circuit potentials in 3.5% NaCl solution. Generally, a more active coating would be expected to cause more hydrogen uptake by the steel and a higher level of re-embrittlement. The influence of coating type on hydrogen re-embrittlement has been discussed in detail in a previous paper [4] and the structure of the coating has been shown to have an important effect, in addition to its electrochemical potential. Etching the coating surfaces in a focused beam of gallium ions (FIB) and examining the resulting trough in a scanning electron microscope revealed the cadmium to have a dense structure, giving better barrier properties. In contrast, the SermeTel 1140/962 coating contained extensive fine pores that are thought to have formed during drying of the inorganic binder in the curing treatment. The pores were mostly closed and, while undesirable, they were less damaging than if they had been through-thickness flaws, which would have left areas of the steel substrate exposed to act as sites where cathodic hydrogen charging would have occurred more readily. The greater porosity of the SermeTel 1140/962 resulted in more hydrogen penetrating this coating than passed through the cadmium. This led to a higher hydrogen concentration at the SermeTel/steel interface, with a higher rate of hydrogen uptake by the specimen and more re-embrittlement. In general terms, the effect of the coating is to determine the hydrogen concentration at the steel surface and the extent of hydrogen uptake and diffusion in the substrate is then the consequence of this concentration.

11

CONCLUSIONS

[1] 300M displayed significant direct embrittlement by hydrogen uptake from electrodeposited cadmium coatings and re-embrittlement from the corrosion of both cadmium and aluminium-based SermeTel 1140/962 coatings. In contrast, AerMet100 showed very little embrittlement in any of these conditions.

[2] The relative embrittlement susceptibilities of the two steels can be explained by their different hydrogen diffusivities, which were measured by the galvanic charging method to be 8.0×10^{-8} and $1.0 \times 10^{-9} \mathrm{cm}^2\mathrm{s}^{-1}$ for 300M and AerMet100, respectively.

[3] The threshold hydrogen concentrations, C_{th}, for propagation of brittle cracks in the two steels were estimated to be in the range 0.4-0.6 of the surface concentration produced by unbaked electrodeposited cadmium.

[4] The greater embrittlement resistance of AerMet100 is attributed to the low rate of hydrogen transport in the reverted austenite phase that forms around martensite laths in its microstructure during tempering. The austenite effectively traps absorbed hydrogen, preventing it being taken up by the more susceptible martensite phase.

REFERENCES

[1] Defence Standard 03-4/2, 'The pre-treatment and protection of steel parts of specified maximum tensile strength exceeding 1450 Nmm^{-2}, 1977.

[2] E. Kossoya, Y. Khoptiara, C. Cytermannb, G. Shemesha, H. Katza, H. Sheinkopfa, I. Cohena & N. Eliaz, 'The use of SIMS in quality control and failure analysis of electrodeposited items inspected for hydrogen effects', Corrosion Science, 50, pp 1481-1491, 2008.

[3] G. Chalaftris & M. J. Robinson, 'Hydrogen re-embrittlement of high strength steel by corrosion of cadmium and aluminium based sacrificial coatings', Corrosion Engineering Science and Technology, Vol. 40, No.1, pp 28-32, 2005.

[4] D.Figueroa & M.J.Robinson, 'The effects of sacrificial coatings on hydrogen embrittlement and re-embrittlement of ultra high strength steels', Corrosion Science 50, pp 1066-1079, 2008.

[5] D. Hardie, E.A. Charles & A.H. Lopez, 'Hydrogen embrittlement of high strength pipeline steels', Corrosion Science, 48, 2006, pp 4378-4385, 2006.

[6] L.W. Tsay, H.L. Lu & C. Chen, 'The effect of grain size and aging on hydrogen embrittlement of a maraging steel', Corrosion Science, 50, 2008, pp 2506-2511, 2008.

[7] J. L.Youngblood & M. Raghavan, 'Correlation of microstructure with mechanical properties of 300M Steel', Metallurgical Transactions A, Vol. 8A, pp 1439-1448, 1977.

[8] R. Padmanabhan & W. E. Wood, 'Microstructural analysis of a multistage heat-treated ultra-high strength low alloy steel', Materials Science and Engineering, No.66, pp125-143, 1984.

[9] B. G. Pound, 'Hydrogen trapping in high strength steels', Acta Materials, Vol.46, No.16, pp5733-5743, 1998.

[10] C.H.Yoo, H.M.Lee, J.W.Chan & J.W.Morris, 'M_2C precipitates in isothermal tempering of high Co-Ni secondary hardening steel', Metallurgical & Metallurgical Transactions A, Vol 27A, pp 3466-3472, 1996.

[11] R.Ayer & P.M.Machmeier, 'Transmission electron microscopy examination of hardening and toughening phenomena in AerMet100', Metallurgical Transactions A, Vol 24A, pp 1943-1955, 1993.

[12] P.Padmanabhan & W.E.Wood, 'Stress corrosion cracking behaviour of 300M steel under different heat treatment conditions', Corrosion, Vol 41, No 12, pp 688-699, 1985.

[13] M.A.V.Devanathan & Z.Stachurski, 'The Absorption and Diffusion of Electrolytic Hydrogen in Palladium', Proc. Royal Soc., A270, pp 90-102, (1962)

[14] C.J.Wen, C.Ho, B.A.Boukamp, I.D.Raistrick, W.Weppner & R.A.Huggins, 'Use of electrochemical methods to determine chemical-diffusion coefficients in alloys: application to LiAl', International Metals Reviews, No 5, pp 253-268, 1981.

[15] P.A.Sundaram & D.K.Marble, 'Hydrogen diffusivity in AerMet100 at room temperature under galvanostatic charging conditions', Journal of Alloys and Compounds, Vol 360, No 1-2, pp 90-97, 2003.

[16] P.A.Sundaram, E.Wessel, H.Clemens, H.Kestler, P.J.Ennis, W.J.Quadakkers & L.Singheiser, 'Determination of the diffusion coefficient of hydrogen in gamma titanium aluminides during electrolytic charging', Acta Mater. 48, pp 1005-1019, 2000.

[17] L.B.Anderson & D.J.Macero, 'Generalised chronopotentiometric potential-time equations and their application to quasi-reversible processes', Analytical Chemistry, Vol 37, No 3, pp 322-326, 1965.

[18] M. J. Robinson & R. M. Sharp, 'The effect of post-exposure heat treatment on the hydrogen embrittlement of high strength steel', Corrosion, Vol. 41, No.10, 582-586, 1985.

[19] T. Yokobori, 'Strength fracture and fatigue of materials', Ed. P. Noordhoff, Groningen, 22-28, 1965.

[20] E. M. K. Hiller & M. J. Robinson, 'Hydrogen embrittlement of high strength steel electroplated with zinc-cobalt alloys', Corrosion Science, Vol. 46, 715-727, 2003.

[21] C.Chatfield, Statistics for technology – a course in applied statistics, third edition, Chapman & Hall, 1983.

[22] C.D.Beachem, 'A new model for hydrogen assisted cracking (hydrogen embrittlement)', Metallurgical Transactions, Vol 3, pp 437-450, 1972.

[23] M.J.Robinson & P.J.Kilgallon, 'Hydrogen embrittlement of cathodically protected high strength, low alloy steels exposed to sulphate-reducing bacteria', Corrosion, Vol 50, No 8, pp 626-635, 1994.

[24] R.P.Gangloff, 'A review and analysis of the threshold for hydrogen environment embrittlement of steel', in Corrosion Prevention and Control, eds M.Levy & S.Isserow, US Army Sagamore Materials Research Conference, 33 (Watertown, MA: US Laboratory Command, 1986), p64.

[25] H.E.Townsend, 'A study of the entry and removal of hydrogen during coating and thermal treatment of steel', Corrosion, Vol 37, No 2, pp 115-119, 1981.

[26] A.Duval & M.J.Robinson, 'Measurement and prediction of hydrogen embrittlement in high strength carbon steel', Corrosion Engineering, Science and Technology. Vol 44, No 5, pp 340-346, 2009.

[27] A.W.Thompson & I.M.Bernstein, 'The role of metallurgical variables in hydrogen-assisted environmental fracture', Advances in Corrosion Science and Technology, Vol 7, Eds. M.G.Fontana & R.W.Staehle, Plenum Press, pp 53-175, 1980.

[28] C.D.Beachem, 'A new model for hydrogen-assisted cracking (hydrogen embrittlement)', Metallurgical Transactions, Vol 3, February, pp 437-450, 1972.

[29] J.Crank, 'The mathematics of diffusion', Second Edition, Oxford University Press, 1975, p 73.

[30] H.S.Carslaw & J.C.Jaeger, 'Conduction of heat in solids', Second Edition, Oxford University Press, 1959, p199.

[31] R.O.Ritchie, M.O.Castro Cedeno, V.F.Zackay & E.R.Parker, 'The effect of silicon additions and retained austenite on stress corrosion cracking in ultra high strength steels', Metallurgical Transactions A, Vol 9A, pp35-40, 1978.

[32] R. L. S. Thomas, D. Li, *et al*, 'Trap-governed hydrogen diffusivity and uptake capacity in ultra high-strength AerMet[®]100 steel', Metallurgical and Materials Transactions, Vol. 33 A, 1991-2004, 2002.

[33] R. L. S. Thomas, J. R. Scully, *et al*, 'Internal Hydrogen Embrittlement of Ultrahigh-Strength AerMet®100 Steel', Metallurgical and Materials Transactions A, Vol. 34 A, No.2, 327-344, 2003.

[34] M.J.Robinson, P.J.Kilgallon & M.Newman, 'Hydrogen embrittlement of cathodically protected duplex stainless steels in seawater containing sulphides', Proceedings 15th International Conference on Offshore Mechanics & Arctic Engineering, Florence, Italy, June 16-20, 1996.

[35] E.Owczarek & T.Zakroczymski, 'Hydrogen transport in a duplex stainless steel', Acta Mater. 48, pp 3059-3070, 2000.

[36] Raghavan Ayar & P.M.Machmeier, 'Transmission electron microscopy examination of hardening and toughening phenomena in AerMet100', Metallurgical Transactions A, Vol 24A, pp 1944-1955, 1993.

ALLOY	Fe	C	Ni	Cr	Si	Mo	V	Nb	Co	Mn
300M	bal	0.4	1.8	0.8	1.6	0.25	-	-	-	0.7
AerMet100	bal	0.23	11.5	3.1	-	-	-	-	13.5	-

Table 1 Compositions (wt %) of 300M and AerMet100 high strength steels

Steel	Diffusion Coefficient $cm^2 s^{-1}$	
	Permeation Method	**Galvanostatic Method**
300M	9.6×10^{-8}	8.0×10^{-8}
AerMet100	-	1.0×10^{-9}

Table 2 Comparison of hydrogen diffusion coefficients for 300M and AerMet100 steels measured by the permeation and galvanostatic methods

	Mean Failure Times (h) & Embrittlement Indices				
	Uncoated	**Cd plated**	**Cd baked**	**Cd corroded**	**Al corroded**
300M	31.6	14.5	30.2	26.6	23.2
(EI)	-	(0.54)	(0.04)	(0.16)	(0.27)
AerMet100	32.9	31.1	32.0	33.8	33.9
(EI)	-	(0.05)	(0.03)	(-0.03)	(-0.03)

Table 3 Mean failure times and embrittlement indices (EI) in the slow strain rate test for 300M and AerMet100 steels in the uncoated condition and after Cd plating, baking and corroding and after coating with SermeTel 1140/962 and corroding.

16
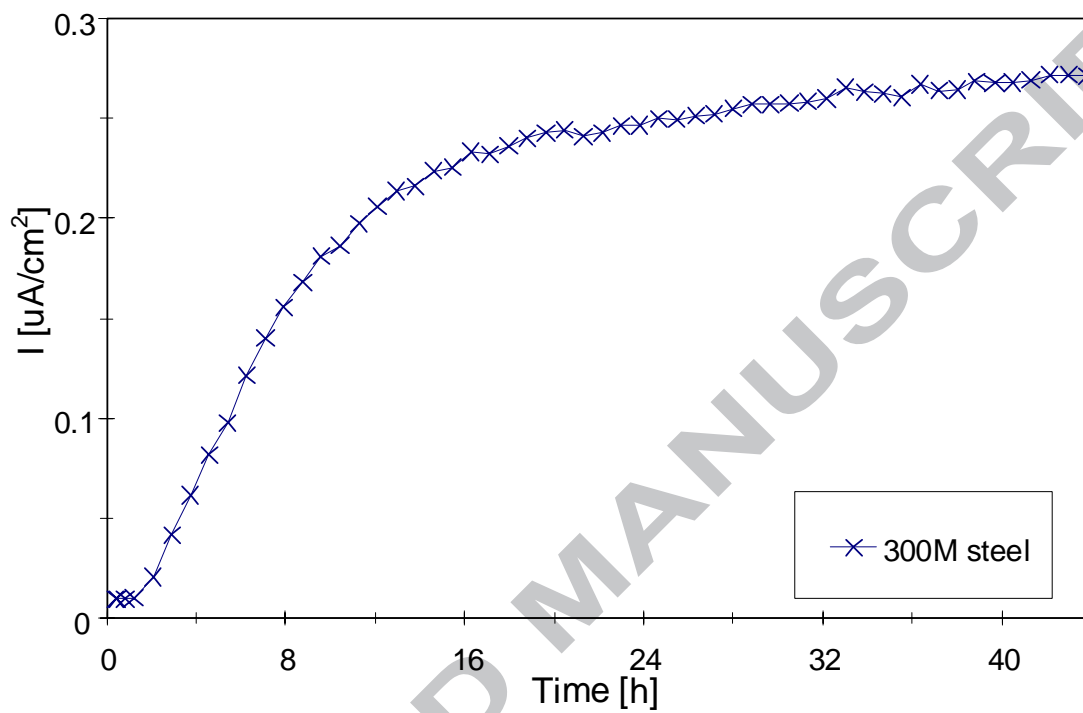
Figure 1. Hydrogen permeation transient for 300M steel charged at -1.25 V (SCE) in 0.2M NaOH solution
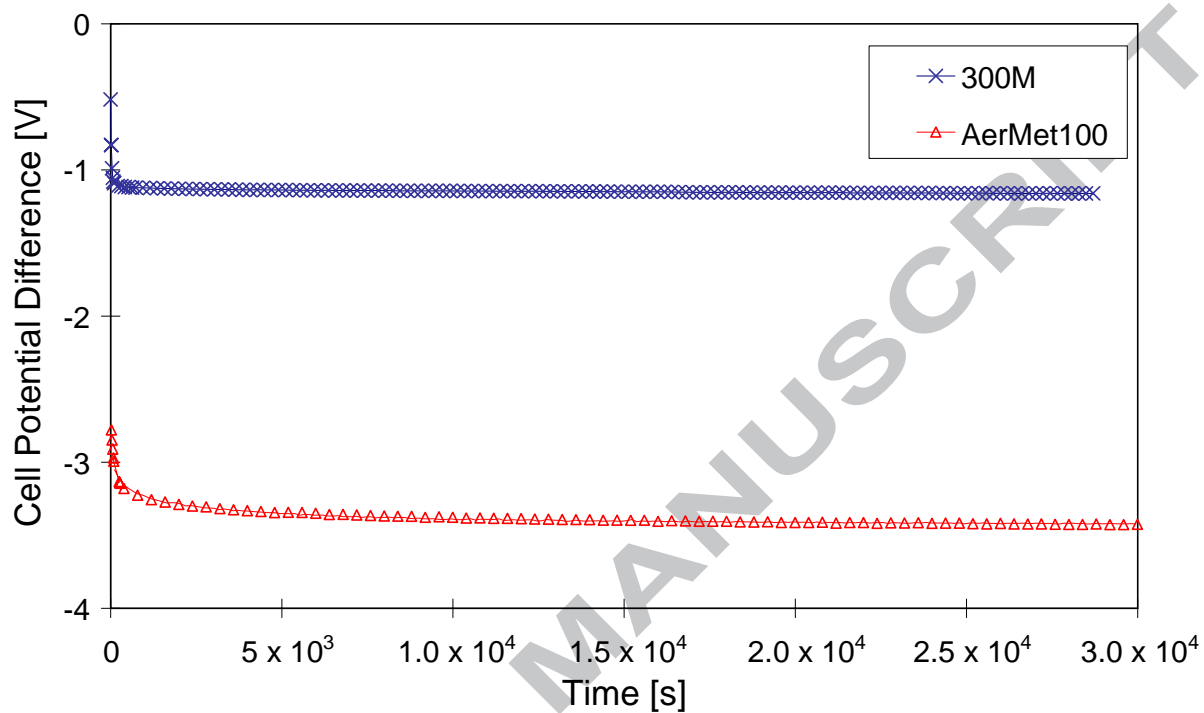
Figure 2. Graphs of cell potential difference versus time obtained for 300M and AerMet100 in the galvanostatic method
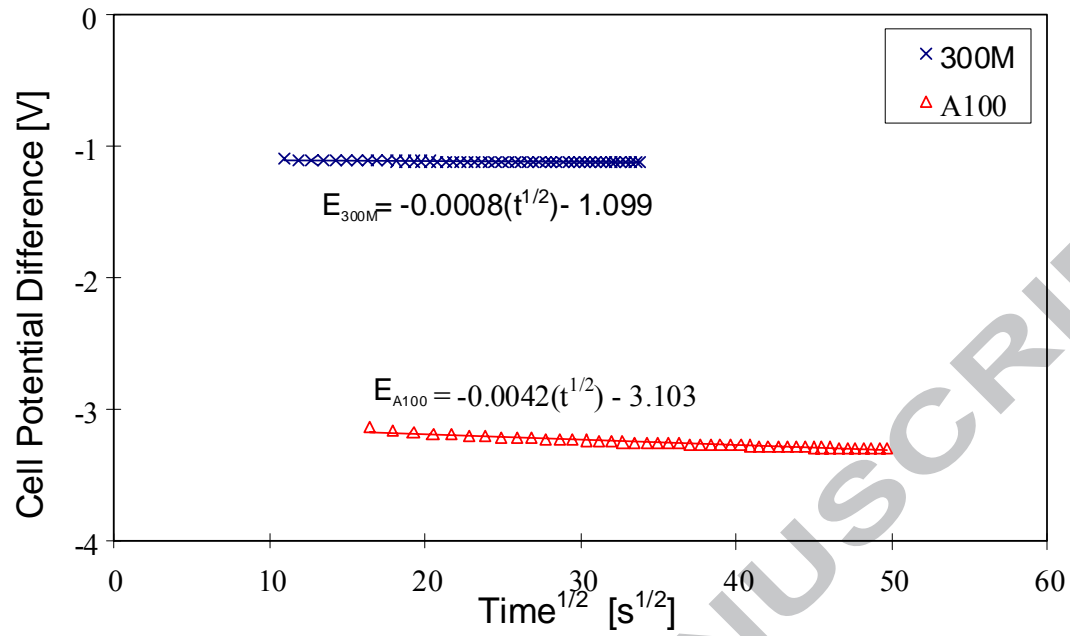
Figure 3. Linear plots of cell potential difference against (time)$^{1/2}$ for 300M and AerMet100 over short charging times ($t \ll L^2/D$)
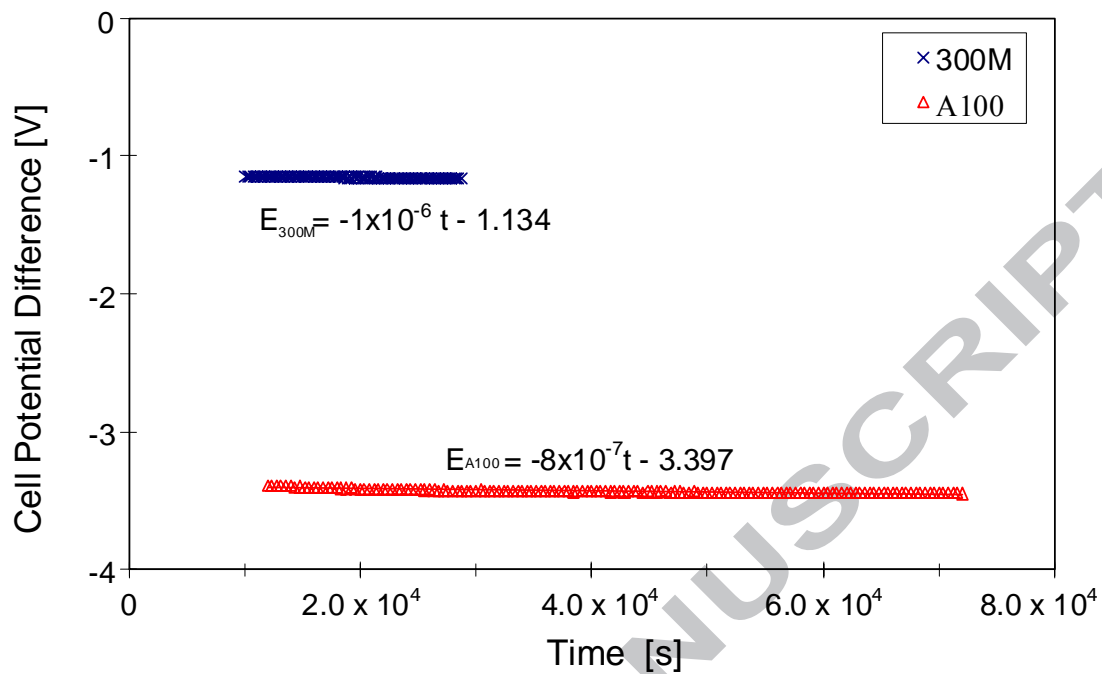
The plot shows Cell Potential Difference [V] on the y-axis (from 0 to -4) versus Time [s] on the x-axis (from 0 to 8.0 x 10^4).

Legend:
- × 300M
- △ A100

$E_{300M}= -1\times10^{-6}\ t - 1.134$

$E_{A100} = -8\times10^{-7}t - 3.397$

Figure 4. Linear plots of cell potential difference against time for 300M and AerMet100 at long charging times *(t >L^2/D)*
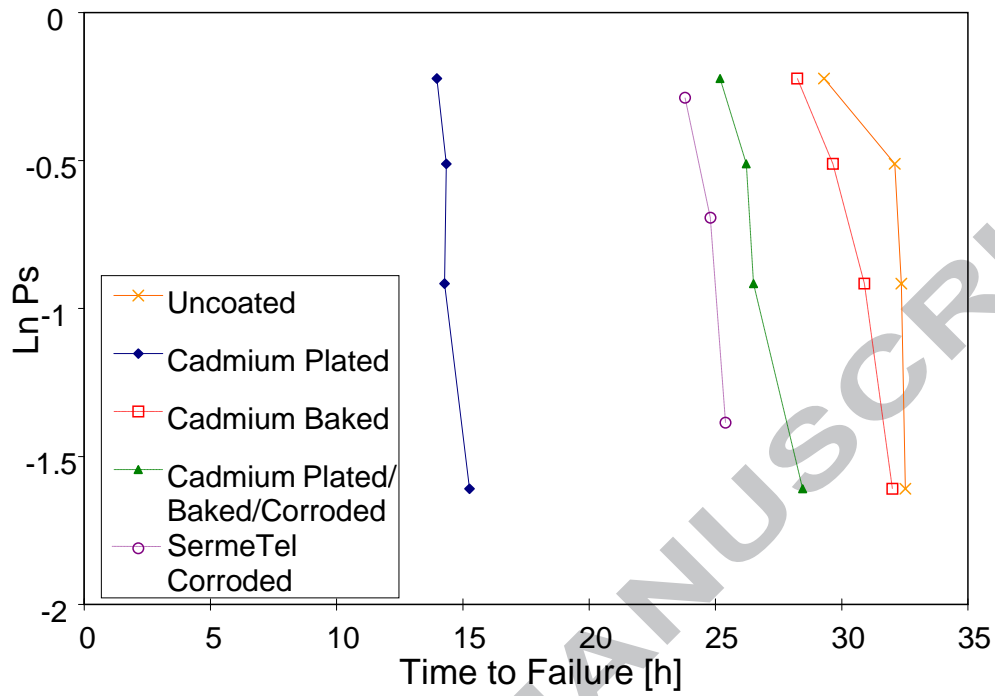
Figure 5. Weibull plots for 300M showing the effects of direct embrittlement from cadmium plating and re-embrittlement from corrosion of cadmium and SermeTel 1140/962 coatings
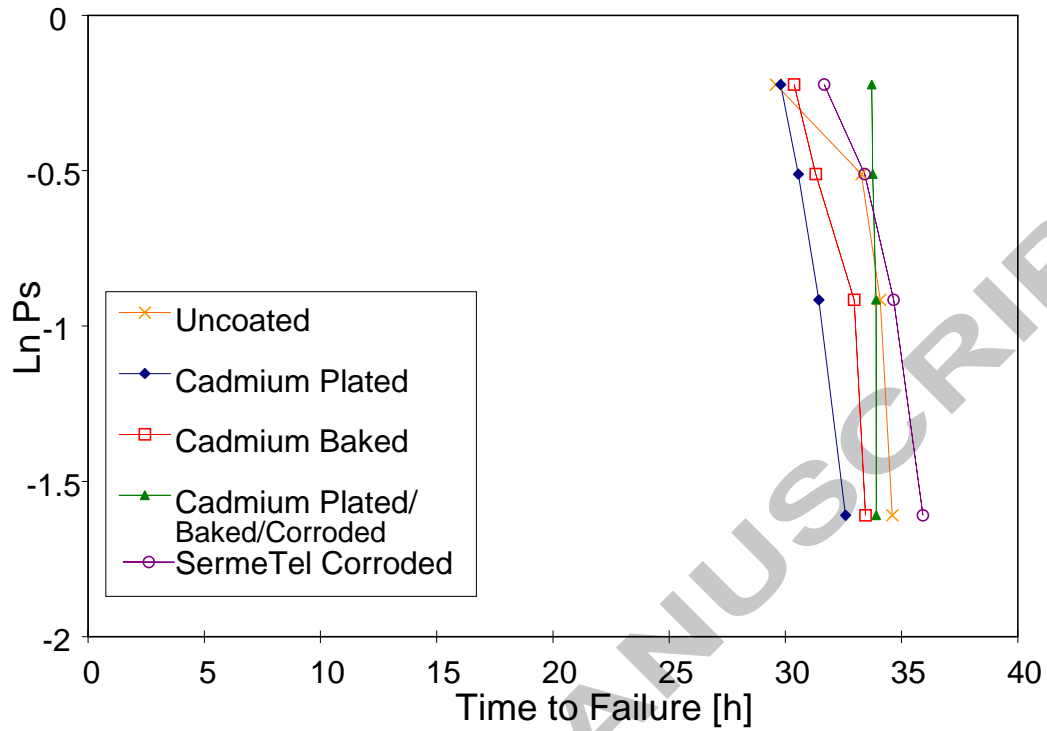
Figure 6. Weibull plots for AerMet100 showing low levels of direct embrittlement from cadmium plating and re-embrittlement from corrosion of cadmium and SermeTel 1140/962 coatings
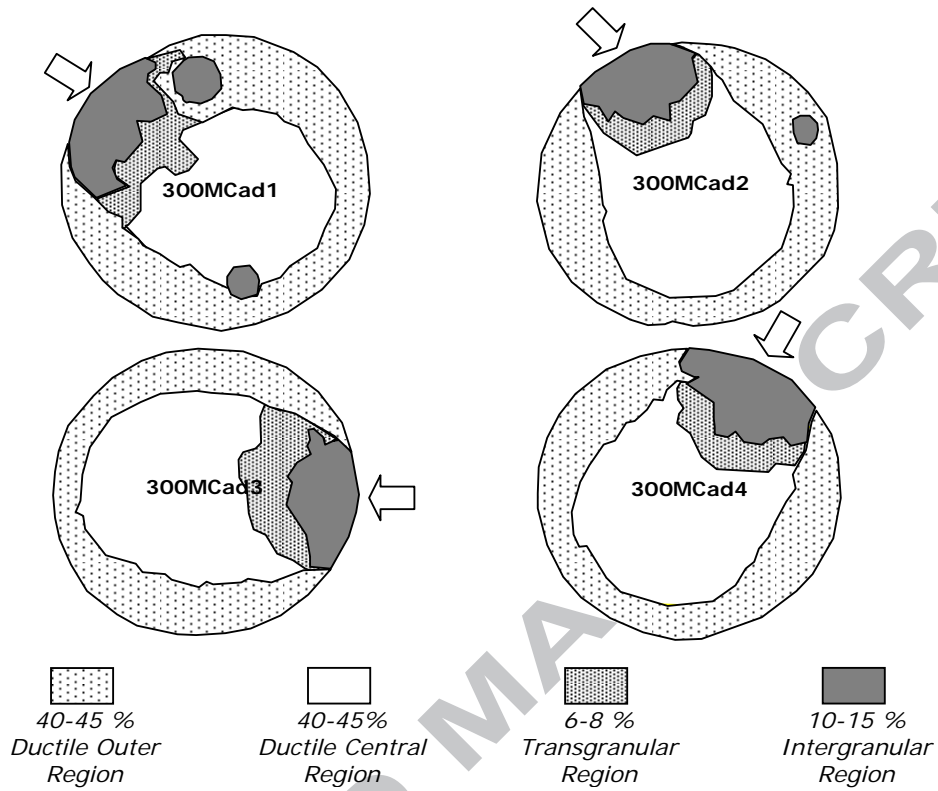
Figure 7. Schematic illustration of different failure modes on the fracture surfaces of four replicate 300M tensile specimens
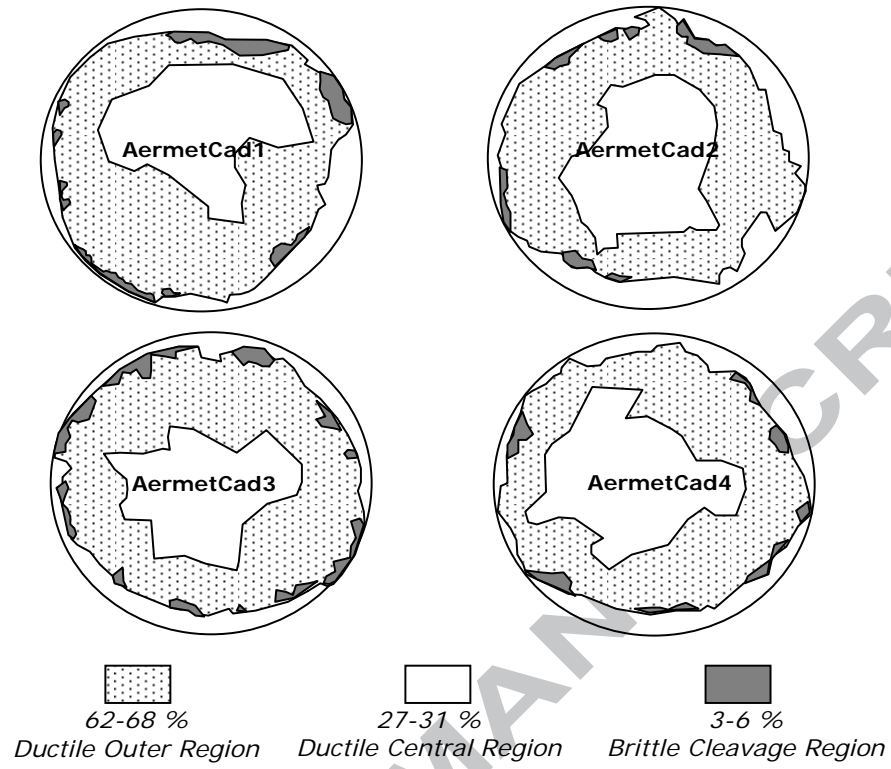
Figure 8. Schematic illustration of different failure modes on the fracture surfaces of four replicate AerMet100 tensile specimens
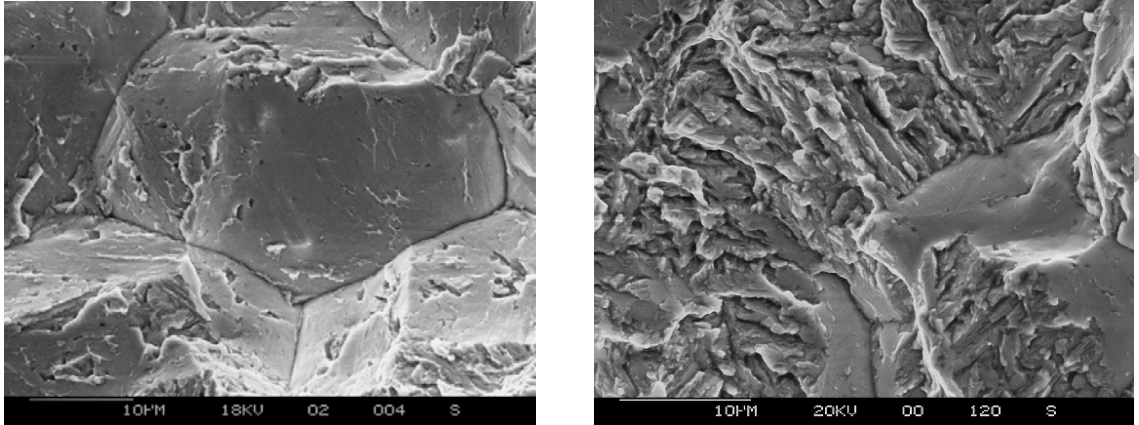
(A)

(B)
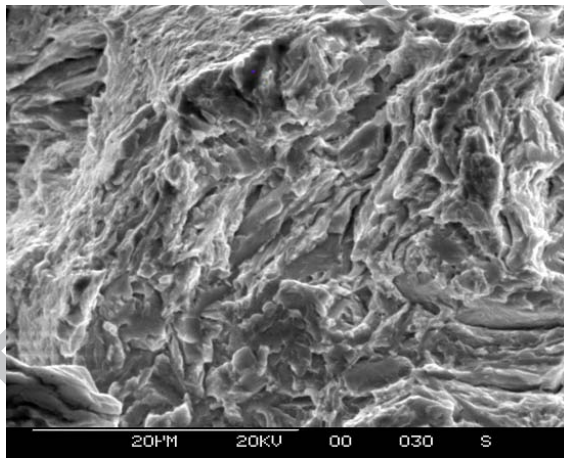
(C)

Figure 9.   SEM Micrographs showing fracture surfaces of cadmium plated slow strain rate specimens. A) brittle intergranular fracture of 300M at prior austenite grain boundaries, B) transgranular fracture of 300M, C) transgranular fracture of AerMet100
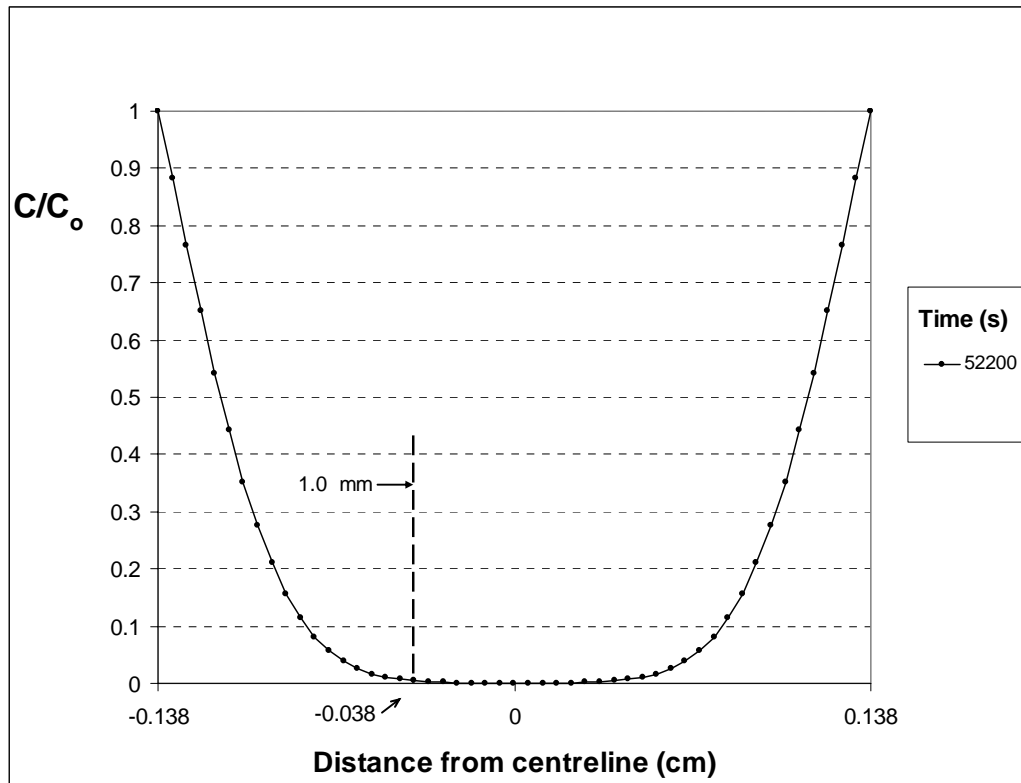
Figure 10. Hydrogen distribution in 300M at the failure time of 14.5h for a diffusivity, *D*, of $1 \times 10^{-8} cm^2 s^{-1}$
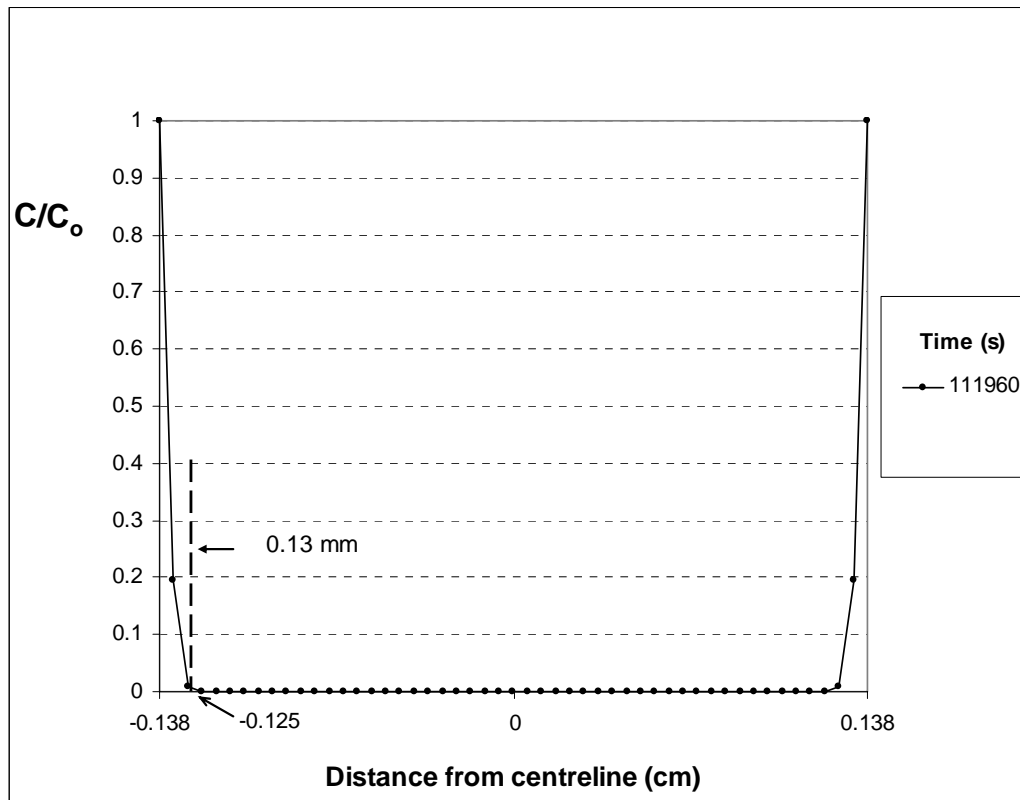
Figure 11. Hydrogen distribution in AerMet100 at the failure time of 31.1h for a diffusivity,D, of $8\times10^{-11}cm^2s^{-1}$
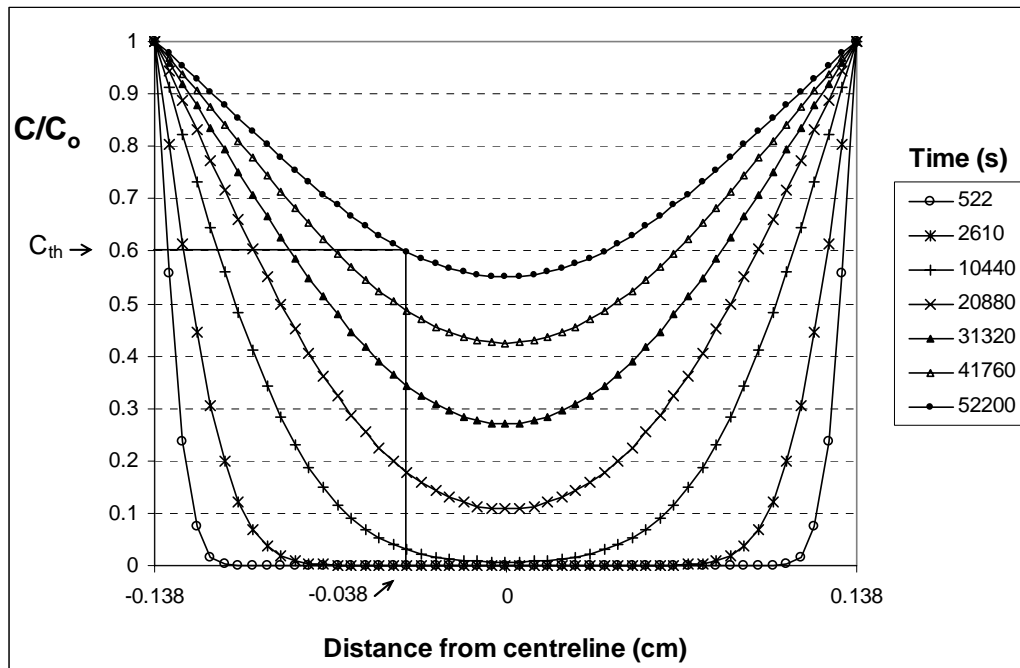
Figure 12. Predicted hydrogen distribution in 300M at the failure time of 14.5h for the measured diffusivity, D, of $8 \times 10^{-8} cm^2 s^{-1}$

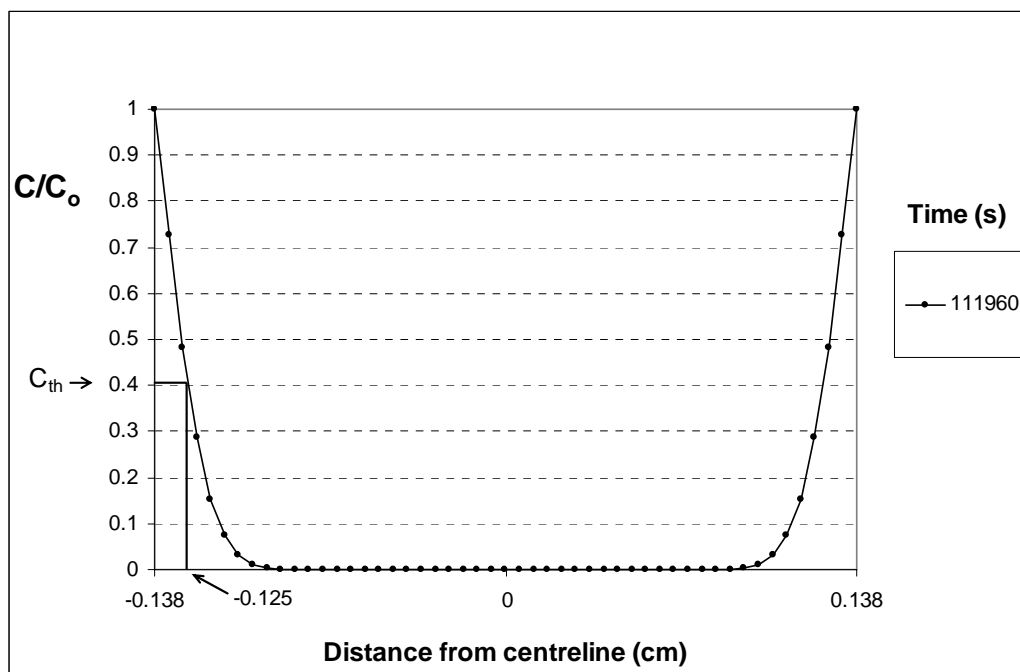**Figure 13. Predicted hydrogen distribution in AerMet100 at the failure time of 31.1h for the measured diffusivity, D, of 1×10^{-9}cm^{2}s^{-1}**
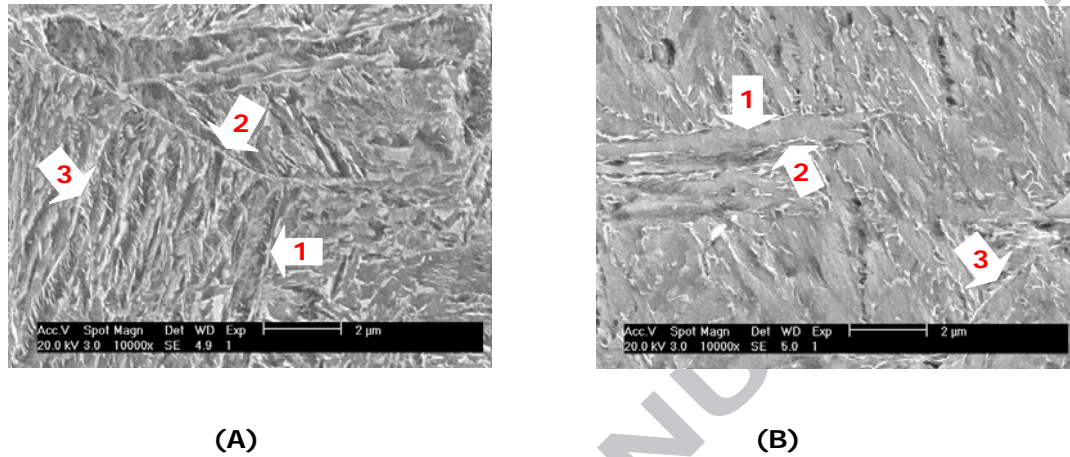
(A)   **(B)**

Figure 14.   SEM micrographs showing A) retained austenite at prior austenite grain boundaries in 300M and B) reverted austenite at lath boundaries (1,2) and at prior austenite boundaries (3) in AerMet 100

30